Aerodynamic Noise Prediction for a Rod-Airfoil Configuration using Large Eddy Simulations

Bharat Agrawal* and Anupam Sharma†

Department of Aerospace Engineering,

Iowa State University, Ames, IA, 50011.

Aerodynamic noise produced by the interaction of wake from a cylinder placed upstream (in tandem) of an airfoil is studied using large eddy simulations (LES). The rod-airfoil interaction problem is a model problem for noise generation due to inflow or upstream-generated turbulence interacting with rotor/stator blades of a turbomachine or a wind turbine. The OpenFoam and Charles (developed by Cascade Technologies) solvers are chosen to carry out the numerical simulations. The airfoil is set at zero angle of attack for the simulations. The flow conditions are specified by the Reynolds number (based on the rod diameter), $Re_d = 48$ K, and the flow Mach number, $M = 0.2$. Comparisons with measured data are made for (a) mean and root-mean-squared velocity profiles in the rod and airfoil wakes, (b) velocity spectra in the near field, and (c) far-field pressure spectra and directivity. Near-field (on- and off-surface data) is used with acoustic analogies (Ffowcs Williams-Hawkings (FW-H) and Amiet's theory[1]) to predict far-field sound.

I. Introduction

Aerodynamic noise is a by-product of most engineering machines, e.g., aircraft, gas turbines, household fans, etc. Aerodynamic noise can be either tonal, in which case the acoustic energy is limited to a few discrete tones, or broadband, in which case the energy is spread across a wide range of frequencies. Flow turbulence is often the source of broadband aerodynamic noise. The wide range of time scales of turbulent eddies results in noise that is produced over a wide range of frequencies. Historically, such broadband noise sources are estimated by using approximate models for the flow turbulence energy spectrum, which is typically scaled using the turbulence kinetic energy and the integral length scale in the problem. These parameters are obtained by solving the Reynolds Averaged Navier Stokes (RANS) equations, which are computationally much less expensive. Large-scale computing that has now become available to researchers, allows direct computation of the full range of length and time scales important for acoustics and hence can get get rid of all the approximations required in simpler models. Direct computation of one such model engineering problem is attempted here using the Large Eddy Simulation (LES) technique.

The problem is to directly compute the noise produced due to aerodynamic interaction between a cylinder and an airfoil (see Fig. 1). A cylindrical rod is placed upstream (in tandem) of the airfoil (NACA 0012). Unsteady wake from the rod convects with the flow and impinges on the downstream airfoil. This interaction produces unsteady lift on the airfoil, which then radiates as noise. At $Re_d = 48,000$, quasi-periodic vortex shedding is expected behind the rod, which gives rise to tones at the vortex shedding frequency and its harmonics. In addition, turbulence in the vortices and the wake generate broadband noise. The resulting noise spectra has a broadband "floor" above which tones with broadened peaks at the shedding frequency and its harmonics are observed. This problem was experimentally investigated by Jacob *et al.*[2] and their results have become the standard against which other researchers have benchmarked their code capability and accuracy. The measurements by Jacob *et al.*[2] contain wake and boundary layer profiles (mean and turbulent statistics), near-field velocity spectra, and far-field noise.

*Ph.D. student, 1200 Howe Hall, bharatr@iastate.edu. AIAA Student Member.

†Assistant Professor, 2341 Howe Hall, Ames, IA, 50011. sharma@iastate.edu. AIAA senior member.

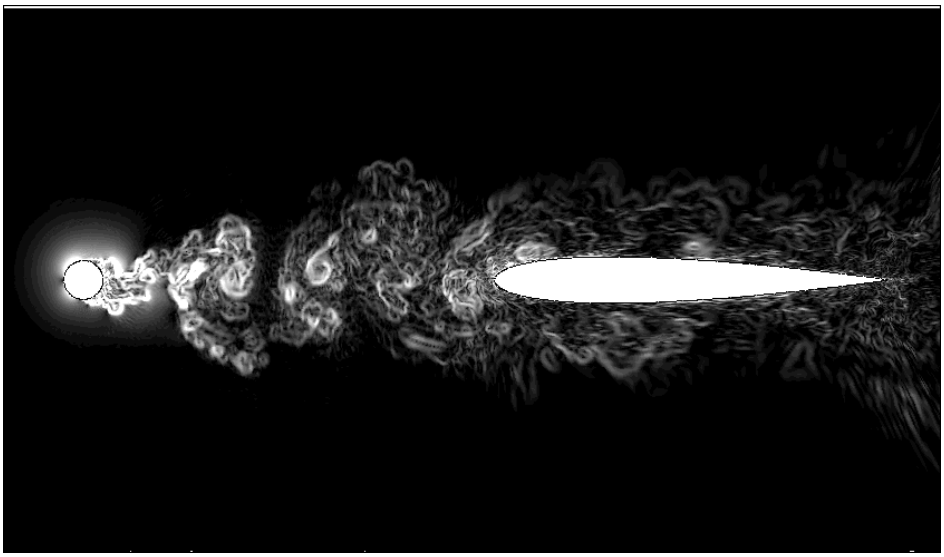

Figure 1: Snapshot of contours of $|\nabla\rho|^{1/4}$ to illustrate the unsteady wake of the rod interacting with the downstream airfoil.

A. Background

A number of numerical studies have been carried out for this specific problem. Casalino *et al.*[3] was first to investigate this problem using unsteady RANS simulations. The simulations were two-dimensional and the three dimensional effects on noise were modeled using a statistical model coupled with the Ffowcs Williams-Hawkings (FW-H) acoustic analogy. The statistical model was calibrated using the experimental data.

The Large Eddy Simulation (LES) technique has been used extensively for this problem. Boudet *et al.*[4] reported the first LES computations for this benchmark problem. It used finite-volume, compressible LES on multi-block structured grids. The acoustics in the far-field was obtained by coupling the near-field data with a permeable FW-H solver.

Berland *et al.*[5] performed direct noise computations for the rod wake-airfoil interaction problem using high-order, compressible LES on overset structured grids. They also investigated the effect on noise of varying the spacing between the rod and the airfoil.

Eltaweel and Wang[6] used an incompressible LES solver coupled with a boundary element method code to predict noise for this problem. An unstructured mesh composing of 22.3 million cells was used. Their results showed very good agreement with data both for near-field flow measurements as well as far-field acoustics.

Giret *et al.*[7] used the unstructured, compressible LES solver, AVBP with a fully unstructured grid to predict the aerodynamics and aeroacoustics of the rod wake-airfoil interaction problem. Far-field noise was predicted using an advanced-time formulation of the FW-H acoustic analogy, which allows simultaneous computation of far-field acoustics with the flow. They used both porous and impermeable (on the rod and airfoil surface) boundaries for evaluating the FW-H boundary integral but found little difference in the predicted noise. They also numerically investigated the effect of offsetting the airfoil in the cross-wise direction by the small amount observed in the experiments. That however did not significantly improve the agreement with the measured wake and velocity profiles.

The present article benchmarks two LES solvers: (a) Charles that solves the compressible flow equations and (b) PisoFoam (OpenFoam) that solves the incompressible flow equations. Near-field data is gathered on the airfoil and rod surfaces and also on a permeable surface surrounding the two geometries. Far-field noise computation is carried out using the FW-H analogy with compressible flow (Charles) data and using Amiet's theory with incompressible flow (PisoFoam) data.

II. Numerical Setup

Figure 2 shows a schematic of the problem. The problem is cast in non-dimensional variables where length is non-dimensionalized by the airfoil chord, velocity by the speed of sound, and density by the freestream density. The rod and the airfoil are placed in tandem along the x direction, the span direction is along the z axis, and the y direction is given by the right-hand rule.

In the experiments by Jacob *et al.*,[2] two different rod diameters were tested. In this article, we focus on the experiment with the rod diameter, $d = 0.1 \times c$, where c is the airfoil chord. Several Reynolds numbers were tested and we limit our focus to $Re_d = 48$ K (based on d) since at that Re, broadband noise contribution is apparent in the data. Separation distance between the rod trailing edge to the airfoil leading edge is $10 \times d$. Two simulations are performed for two different airfoil angles of attack - 0 and 10 degrees. The zero degree angle-of-attack case is the primary focus as experimental data is only available for that case. The 10^0 case is used to numerically investigate the effects of airfoil loading on radiated noise. Jacob *et al.*[2] note that in the measurements for the zero-degree case, the airfoil was perhaps at a slight ($\sim 2^0$) angle of attack, and slightly offset in the y direction. These geometric anomalies are not incorporated in the numerical model.

Figure 3 shows a close-up cross-sectional view of the grid. The computational boundaries in the x and y direction are taken to be between 10-15 airfoil chords away from the bodies. Even though the geometry is essentially 2-D (extruded in the third, span-wise dimension), instantaneous turbulent flow over these bodies is three dimensional, and the computational domain has to be 3-D as well. However, simulating the entire span-wise length (as in the experiment) is computationally very expensive and usually not required. Periodic boundary conditions can be employed in the span-wise direction if the domain is larger than the largest eddy size along the span. Span-wise spatial coherence provides a measure of the largest eddy size and this information is used from the measured data to restrict the LES domain size to one airfoil chord in the span direction.

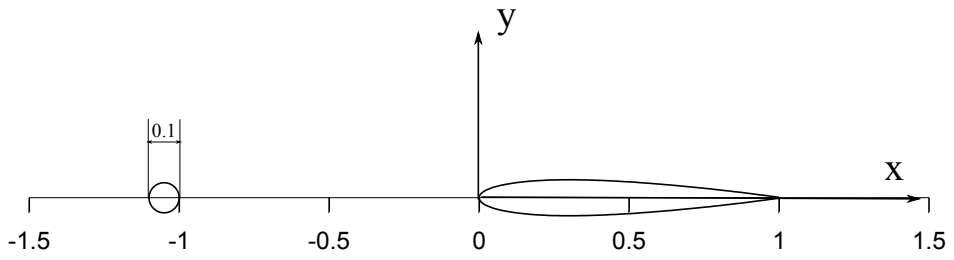

(a) 2-D Schematic

Figure 2: Schematic showing the non-dimensional size and positions of the rod and the airfoil.

A fully structured, multi-block grid is used and the blocking topology can be inferred from Fig. 3. Gridgen (from Pointwise Inc.) is used to generate the grids. An O-grid is used around the rod and a C-grid around the airfoil to efficiently resolve the boundary layers on the bodies. The grid is stretched geometrically away from the surfaces (in surface-normal direction) until unit aspect ratio is reached. Beyond this, the grid is kept uniform in the region where the rod wake turbulence is expected. Outside of this region, the grid is again geometrically stretched till the farfield boundary.

The blocking and the grid density are designed to resolve: (1) the turbulence in the rod wake in the gap region, (2) the boundary layer on the rod, and (3) the boundary layer on the airfoil. The first cell height on the airfoil and the rod are chosen such that $y^+ = \dfrac{y}{\nu\sqrt{\rho/\tau_w}} = 1$, where ν is the fluid kinematic viscosity, τ_w is the wall shear stress, and ρ is the fluid density. This is a very conservative estimate, since such small first cell height is required for resolving wall boundary layers. The problem under investigation is the interaction of turbulence in the rod wake with the airfoil, hence accurate resolution of the turbulence generated by the airfoil is not of paramount importance. This conservative approach was still taken however with the intent that in the future, the same grid could be used to study "self" (trailing edge) noise from this airfoil and a comparison could be made between "self" noise and inflow (coming from rod wake) turbulence noise.

Full description of the OpenFOAM and Charles solvers will be provided in the final paper.

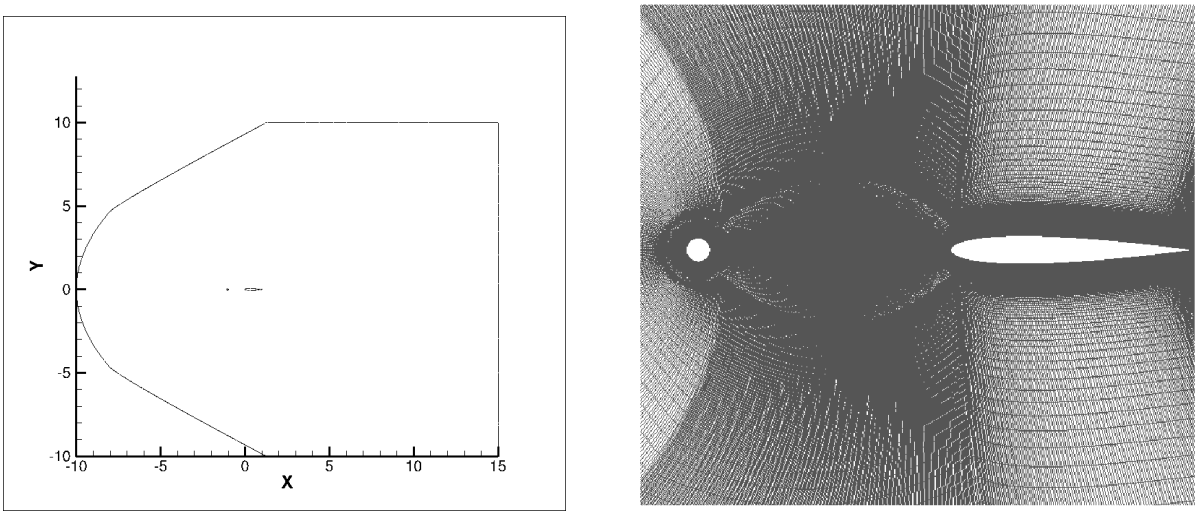

(a) Computational Domain

(b) Zoomed-in view

Figure 3: Cross-sectional $(x - y)$ views of the computational domain and the grid around the rod and the airfoil.

III. Results and Data Comparisons

The measurement data includes mean and r.m.s. velocity profiles at various locations ahead of and behind the airfoil, near-field velocity spectra, as well as far-field acoustic spectra and directivity. Comparisons against these measurements for the zero-degree AoA case are systematically presented in this section.

A. Meanflow

The phenomena of interest in the problem under investigation are unsteady, but statistically stationary. The interest is not in *transient* phenomena such as instantaneous/impulsive start of the rod/airfoil combination. In the experiments, the wind tunnel is started and the rig is allowed to reach a statistically stationary state before measurements are taken. Similarly, the computations have to reach a statistically stationary state before any unsteady data can be gathered from the simulations. Removal of initial transients from the computational domain is therefore required before meaningful results can be sampled. We initialize the flowfield using a 2-D RANS solution. The flow is then evolved for about 20 time units, which is tantamount to the flow going past the airfoil about 4 times. The time period of wake shedding from the cylinder for $Re_d = 48$ K is 2.5 time steps. The simulations are run for 8 wake shedding periods to get rid of the transients.

1. *Mean and R.M.S. Velocity Profile Comparisons*

The mean and the r.m.s. velocity profiles were measured at various axial locations (stations). These stations are specified in terms of the axial distance non-dimensionalized by the airfoil chord. Figure 4 shows the locations of these stations in the domain. In order to compare the measured profiles against the predictions,

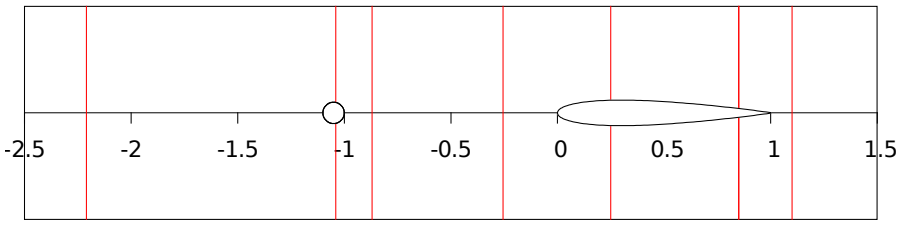

Figure 4: Axial locations (shown by red lines) where mean and r.m.s. wake/velocity comparisons are made.

time-accurate data has to be collected over several periods (of wake shedding) and then processed to get the mean and the r.m.s. values. For the comparisons shown in Fig. 5, the data was sampled for 4 periods of wake shedding. Little difference in profiles was observed when compared with data sampled over fewer (3) periods. When comparing the results in Fig. 5, the reader should bear in mind two key differences between the experiment and the simulation: (1) in the experiment, the airfoil is slightly offset in the positive y direction by a distance of about 2% chord, and (2) the airfoil is at a slight angle-of-attack (around 2^o). These make the measured profiles slightly asymmetric, whereas the predicted profiles are symmetric.

Figure 5 (a & b) show the mean and the r.m.s. axial velocity upstream of the rod (essentially showing the freestream conditions). The data shows a very slight incoming turbulence intensity, which is identically zero in the simulations. Figure 5 (c & d) plot the profiles on the rod slightly past the peak C_p point. The data was collected above the rod (positive y). Flow acceleration due to rod thickness and development of the boundary layer (as seen in u_{rms} profile) are captured by both solvers. The reason for non-zero turbulence intensity in OpenFoam away from the rod is being investigated currently.

Figure 5 (e & f, and g & h) show the profiles between the rod and the airfoil. (at $x/c = -0.87$ and $x/c = -0.255$). Very large discrepancy in the mean velocity is observed in Fig. 5 (e) and the authors are suspicious of the mean velocity data at this station. The peak velocity deficit in the wake is expected to reduce with distance away from the rod, however the measured mean velocity profiles in Fig. 5 (e & g) show the peak velocity deficit increasing with downstream distance! Some discrepancy however can be attributed to numerics as well - the simulations consistently over-predict u_{rms} (a measure of turbulence intensity). Fig. 5 (g) starts to reflect the slight asymmetry in the experiments; the peak velocity deficit appears to be at $y/c > 0$. Jacob *et al.*[2] asserts that this slight asymmetry does not affect the far-field noise and hence no attempt was made to simulate these geometric asymmetries.

Velocity profiles in Fig. 5 (i & j, and k & l) were also measured only on one side of the airfoil (positive y). The velocity profiles on the airfoil are determined by the rod wake turbulence (due to the high intensity and length scale) rather than the development of the airfoil boundary layer. Hence the errors accumulated in the simulations upstream of the airfoil are also reflected in these comparisons.

In general the mean velocity deficit and r.m.s. velocity predicted by the two solvers are in very good agreement. Both however over-predict the mean velocity deficit and the r.m.s. velocity. This is interesting because the two solvers use very different sub-grid models. The Vreman[8] model is used with Charles whereas the dynamic Smagorinsky model is used with PisoFoam. More discussion and analyses of these results will be presented in the final paper.

B. Near-field Velocity Spectra

While comparing the mean and r.m.s. velocity profiles help in assessing flow prediction accuracy, the interest is in predicting radiated noise, which has its sources in the turbulence spectra. Measurements are available of near-field power spectral density at a few locations close to the airfoil. Power spectral density is defined as the magnitude of the Fourier transform of the autocorrelation of a variable (here chosen to be axial velocity). The autocorrelation function, $R_{uu}(\tau)$ is defined as

$$R_{uu}(\tau) = \lim_{T\to\infty} \frac{1}{T} \int_0^T u(t)u(t+\tau)\ \mathrm{d}t, \tag{1}$$

and the power spectral density (PSD), $S_{uu}(\omega)$ as

$$S_{uu}(\omega) = \int_{-\infty}^{\infty} R_{uu}(\tau)\ \exp(-i\omega\tau)\ \mathrm{d}\tau. \tag{2}$$

Note that u is dimensionless and hence $R_{uu}(\tau)$ is dimensionless, while $S_{uu}(\omega)$ has the dimension of time (or 1/frequency). PSD is therefore written as per Hz or per Strouhal number, St. PSD may also be calculated directly as

$$\begin{aligned} S_{uu}(\omega) &= E|\hat{u}(\omega)|^2 \\ &= \frac{1}{T} \int_0^T u^*(t) \exp(i\omega t)\ \mathrm{d}t \int_0^T u(t') \exp(-i\omega t')\ \mathrm{d}t'. \end{aligned} \tag{3}$$

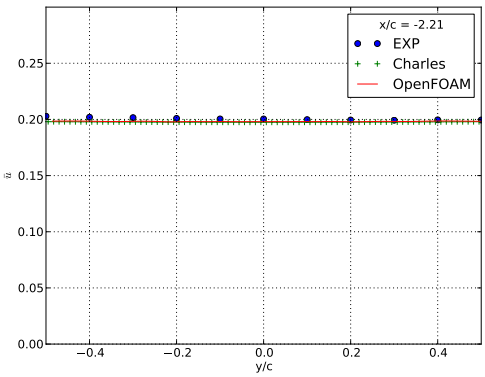

(a) $\bar{u}/c_0$ at $x/c = -2.21$

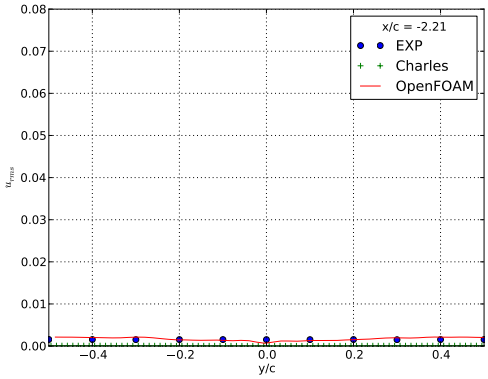

(b) u_{rms}/c_0 at $x/c = -2.21$

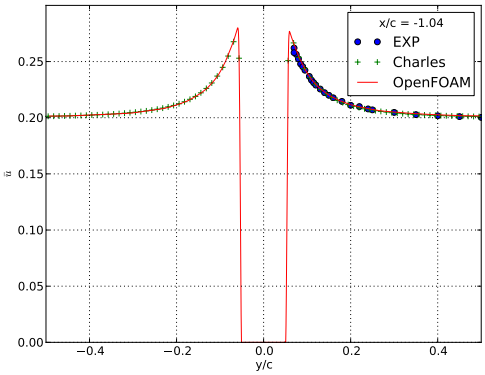

(c) $\bar{u}/c_0$ at $x/c = -1.04$

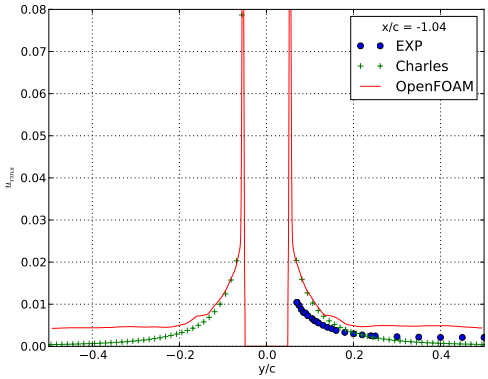

(d) u_{rms}/c_0 at $x/c = -1.04$

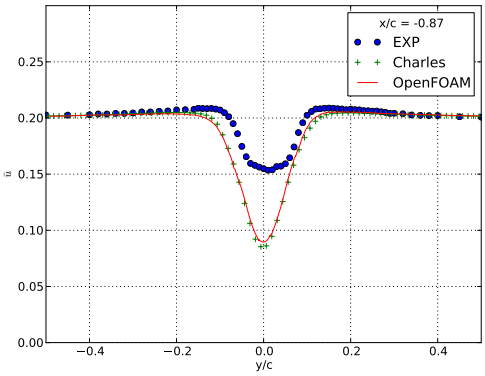

(e) $\bar{u}/c_0$ at $x/c = -0.87$

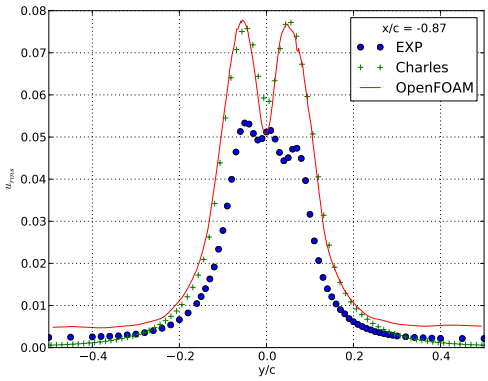

(f) u_{rms}/c_0 at $x/c = -0.87$

Figure 5: Mean and r.m.s. velocity comparisons between data and predictions.

The PSD For a discrete series, u_n with $1 \leq n \leq N$, is obtained using

$$S_{uu}(\omega) = \frac{(\delta t)^2}{T} \left| \sum_{n=1}^{N} u_n \exp(-i\omega\, n\delta t) \right|^2. \tag{4}$$

This is typically averaged over multiple samples to reduce statistical scatter in predicted spectra. Near-field velocity spectra are compared against measurements at two points indicated by "A" and "B" in Fig. 6. The

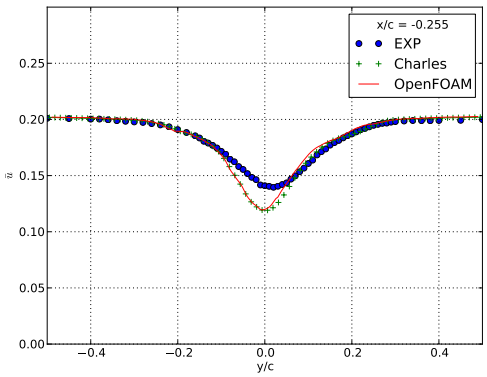

(g) $\bar{u}/c_0$ at $x/c = -0.455$

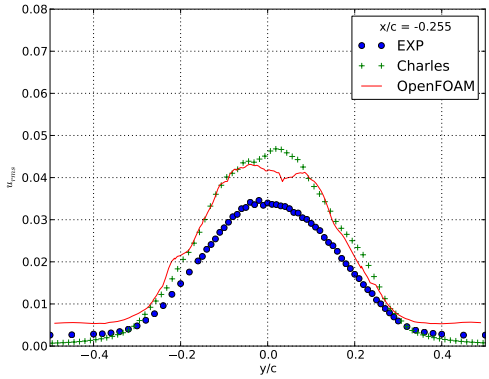

(h) u_{rms}/c_0 at $x/c = -0.455$

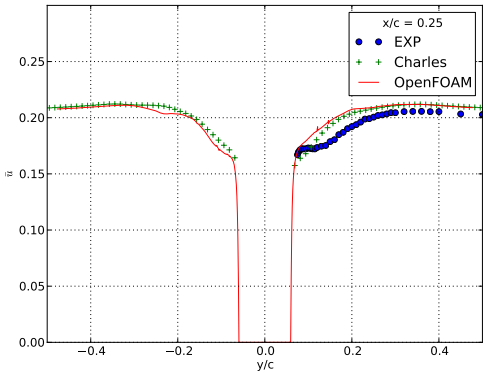

(i) $\bar{u}/c_0$ at $x/c = 0.45$

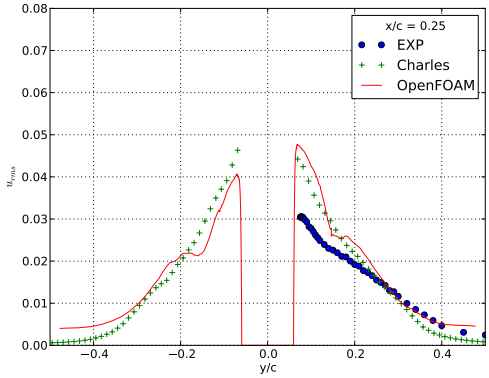

(j) u_{rms}/c_0 at $x/c = 0.45$

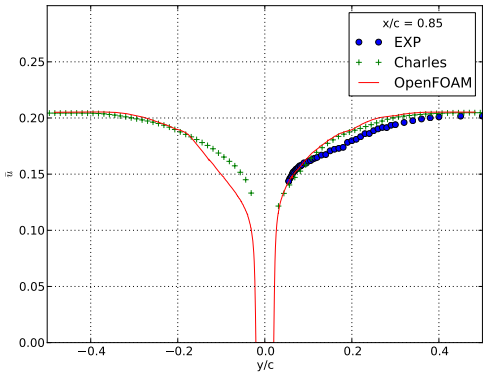

(k) $\bar{u}/c_0$ at $x/c = 0.85$

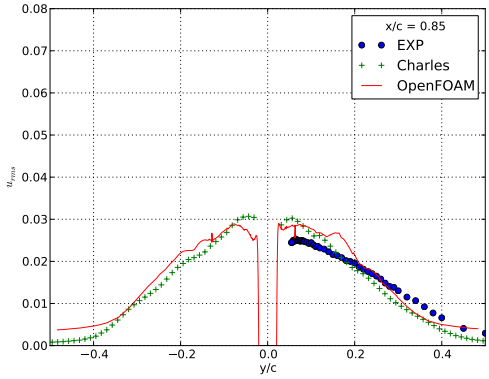

(l) u_{rms}/c_0 at $x/c = 0.85$

Figure 5: (Continued) Mean and r.m.s. velocity comparisons between data and predictions.

plots in Fig. 7 show the velocity power spectral density comparisons at points "A" and "B". Numerical data was gathered for a total of 57.5 time units, which is equivalent to 23 periods of wake shedding. The data was divided into 5 samples with an overlap of 50%, and the PSD computed for each sample. Final spectrum is obtained by averaging the PSDs over these 5 samples. The resolution in the predicted spectra is less than desirable, however two essential features of the spectra - (1) the spectral peak amplitude at $St \sim 0.2$, and (2) the spectral decay beyond the spectral peak, are captured reasonably well by the predictions. The scatter in the predicted spectra is due to the relatively few (5) samples over which averaging is performed.

Computational cost limits how long the simulation can be run, and hence the number of samples over which the spectra can be averaged. The same length (in time) of data could be split up into more samples and the scatter reduced by averaging over increased number of samples, however that would reduce the frequency resolution further and also the lowest resolved frequency would increase.

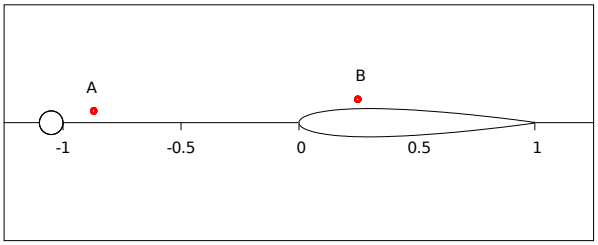

Figure 6: Locations denoted by "A" and "B" at which near-field spectra comparisons are made.

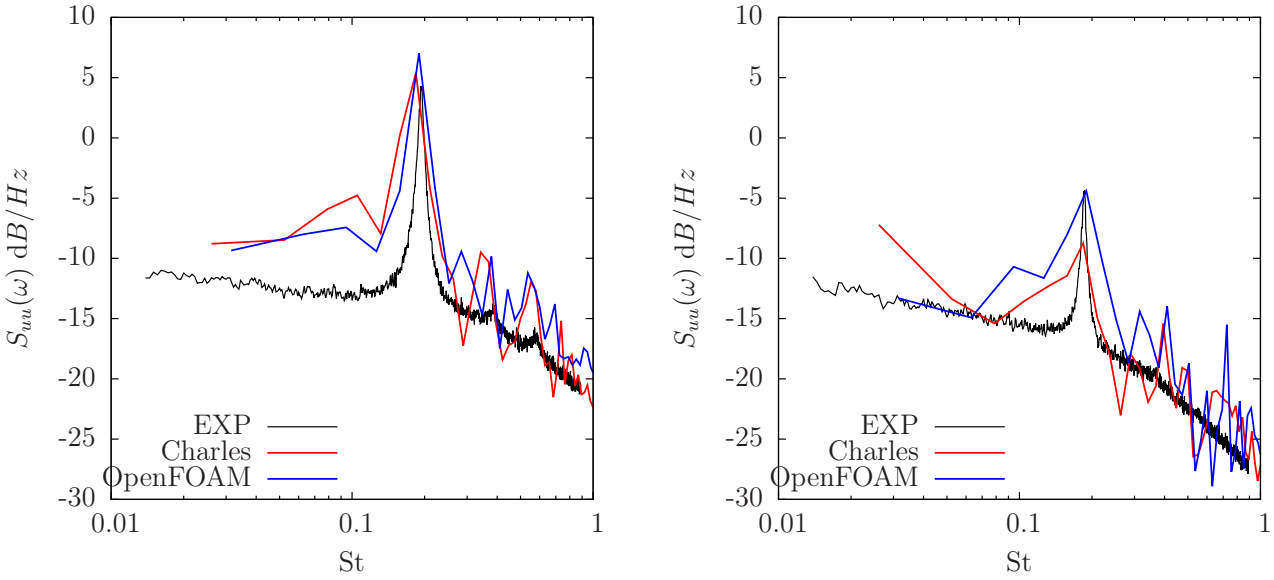

(a) Spectra at point "A": $x/c = -0.87$, $y/c = 0.05$

(b) Spectra at point "B": $x/c = 0.25$, $y/c = 0.1$

Figure 7: Velocity power spectral density, $S_{uu}(\omega)$ dB/Hz, plotted against Strouhal number at points "A" and "B" shown in Fig 6.

C. Far-field Spectra

Two different approaches are required to predict far-field noise. The compressible, time-accurate data in the near-field obtained from Charles is used directly with a FW-H solver. For the incompressible solution obtained using PisoFOAM, Amiet's[1] theory will be used to predict noise in the farfield. Results from solving the FW-H equation with the Charles data are presented below. OpenFOAM results will be overlaid on these and discussed in the final paper.

Time accurate data is collected on a surface, Σ, enclosing all the noise sources. The integral equation derived by Ffowcs Williams and Hawkings (FW-H), Eq. 5, is then solved to obtain acoustic pressure in the far-field. Eq. 5 is a reduced form of the full FW-H equation obtained by ignoring the volume source term. In this problem (due to the small flow Mach number) the noise sources are primarily the unsteady lift on the airfoil and the rod. The contribution to far-field noise from off-surface (quadrupole) sources is expected

to be insignificant.

$$\begin{aligned} 4\pi|\mathbf{x}|p'(\mathbf{x},t) &= \frac{x_i}{c|\mathbf{x}|}\frac{\partial}{\partial t}\int \left[p' n_i + \rho u_i (u_j - U_j) n_j\right] \, \mathrm{d}\Sigma \\ &+ \frac{\partial}{\partial t}\int \left[\rho_0 u_i + \rho'(u_i - U_i)\right] n_i \, \mathrm{d}\Sigma. \end{aligned}$$

The FW-H equation solver available with the Charles suite of codes is used for far-field noise prediction. During the execution of Charles, time accurate data was sampled on the following surfaces: (1) one surface enclosing both the airfoil and the rod, (2) individual surfaces enclosing the rod and the airfoil separately. In the end the single surface (enclosing both the rod the airfoil) was used for all noise predictions (see Fig. 8).

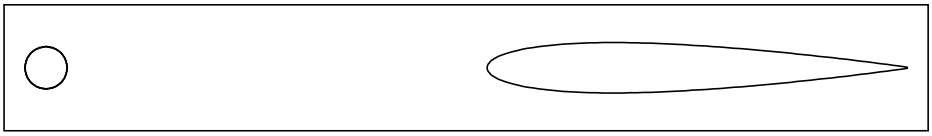

Figure 8: FW-H integration surface for calculating far-field noise. A permeable surface surrounding both the rod and the airfoil together is selected.

As mentioned earlier, the CFD domain in the span-wise direction is typically a small fraction of the span of the experimental model. One therefore cannot directly compare the measured versus the predicted far-field noise. The correction that needs to be applied to the predicted spectra depends on span-wise coherence. If we denote span-wise coherence length by L_c and use subscripts $(\,)_s$ for simulations and $(\,)_e$ for experiments, then Eq. 6 can be used for comparing measured and predicted spectra.

$$\begin{aligned} \left(S_{pp}(\omega)\right)_e &= \left(S_{pp}(\omega)\right)_s + 20\log\left(L_e/L_s\right) \;\forall\; L_s < L_c, \\ \left(S_{pp}(\omega)\right)_e &= \left(S_{pp}(\omega)\right)_s + 10\log\left(L_e/L_s\right), \;\forall\; L_s > L_c, \\ \left(S_{pp}(\omega)\right)_e &= \left(S_{pp}(\omega)\right)_s + 20\log\left(L_c/L_s\right) \\ &+ 10\log\left(L_e/L_c\right) \;\forall\; L_s < L_c < L_e. \end{aligned} \tag{5}$$

Equation 6 assumes that over span-wise length L_c, there is perfect correlation which drops identically to zero outside of this region. This 'box-car' simplification by Kato[9] is often used and is employed here.

The span length (of the rod and airfoil assembly) is ten times the rod diameter (which is one-third of the span length of the model used in the experiment). The span-wise coherence observed at the peak Strouhal number (where the coherence is expected to be largest) is about 0.75 times the rod diameter in the measured data. Since $L_{sim} > L_c$, the correction needed is

$$\begin{aligned} \left(S_{pp}(\omega)\right)_{s\ corr} &= \left(S_{pp}(\omega)\right)_s + 10\log\left(L_e/L_s\right), \text{ or,} \\ \left(S_{pp}(\omega)\right)_{s\ corr} &= \left(S_{pp}(\omega)\right)_s + 10\log\left(3\right). \end{aligned} \tag{6}$$

Figure 9 compares the predicted (with the span correction) far-field pressure spectral density against the data measured at a point directly above the airfoil leading edge at a distance of 18.5 airfoil chords. A total of approximately 30 time units of data (equivalent to 12 wake shedding periods) was sampled. Noise is computed with the same exact data using five different sample sizes. The data is divided into n segments (where n is varied from 1 to 5). Noise is predicted from each sample individually, then far-field pressure squares averaged over n samples (assuming fully uncorrelated data) to get the final noise signature. Samples with overlapping data are used, where the overlap length is taken to be 50% of the sample/segment length.

Fig. 9 shows a comparison between the data and the prediction of far-field pressure spectral density using five different sample sizes. Keyword "#samp n" refers to the sampling procedure in which the entire data is divided into n segments (partially overlapping). As the number of samples increase, the net time duration captured by the data reduces. This reduces the frequency resolution in the predicted spectrum. While for small number of samples, the increased frequency resolution comes at the cost of high scatter in the predicted spectrum.

The agreement between the measured and the predicted spectra in Fig. 9 is good, however, the need for longer time data is apparent. The spectral peak (at shedding frequency) is captured well but the frequency spread of the peak and the spectral broadening are comparable to data only in the magenta and blue curves, which have relatively large scatter. Simulations with longer (almost 2-3 times) time data are needed to convincingly say that the spectral peak broadening is quantitatively captured by the simulations. Nevertheless, the simulations clearly capture the spectral decay with increasing frequency, which indicates that some aspects of broadband noise are accurately captured by the prediction methodology.

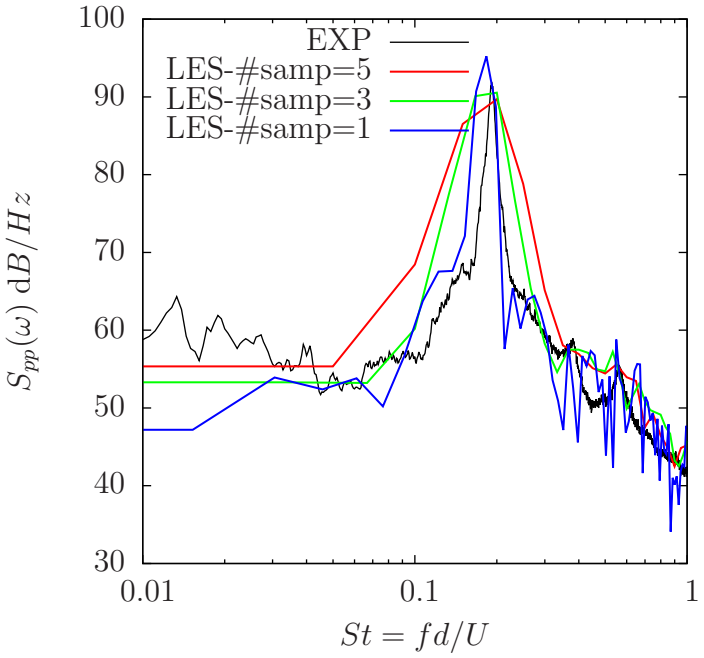

Figure 9: Far-field pressure spectral density directly above the airfoil leading edge ($\theta = 90^0$) at a distance of 18.5 chords. Three different predictions (with varying number of samples used for averaging) are plotted.

Predicted and measured directivities of the peak noise frequency (wake shedding frequency) are compared in Fig. 10. In making the comparison, the measured data (microphone angles) has been corrected (using Amiet's correction) for refraction due to the shear layer present in the experiment. The overall shape is captured with generally better agreement between the data and the prediction for downstream angles. Little variation is observed between predictions using different number of samples.

IV. Conclusions

Some inferences are drawn based on current results. More results and final conclusions will be presented in the full paper.

Two different LES solvers Charles and OpenFoam are used to predict aerodynamic noise due to rod wake-airfoil interaction. Mean and r.m.s. velocity profiles, near-field velocity spectra, and far-field acoustic pressure spectra and directivity are compared between predictions and measurements. The meanflow comparisons show good agreement between the solvers but the agreement with the measured data is moderate. Velocity deficit and turbulence intensity in the wakes are generally over-predicted by the solvers. In terms of spectra comparisons (both near- and far-field), the overall levels, tonal peak, and spectral fall off is captured by the predictions. The directivity comparisons made only for the peak Strouhal number, show very good agreement with data.

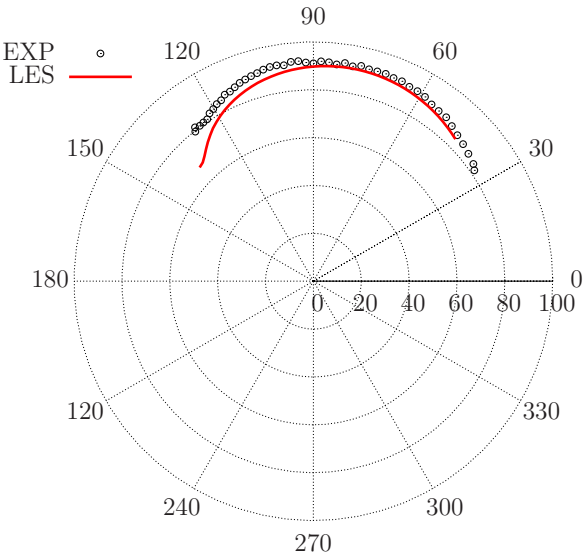

Figure 10: Directivity of the peak acoustic pressure (spectral density plotted at $St = 0.2$). The polar angle (values listed on the periphery of the plot) is measured from upstream.

V. Acknowledgment

The authors thank the General Electric Global Research Center for sponsoring this research as well as for arranging for computer time at the Brookhaven National Laboratory computers. Many fruitful discussions with Drs. Lawrence Cheung, Giridhar Jothiprasad, and Umesh Paliath without which this project would not have succeeded, are acknowledged. Thanks are also due to Dr. Anne Dord for some help with the Charles solver. The computations used to produce the results in this report were conducted using computing resources provided by Brookhaven National Laboratory, Argonne National Laboratory, and NSF XSEDE. The author would like to acknowledge their support. Partial support from the Iowa NASA EPSCoR program is also acknowledged.

References

[1]Amiet, R. K., "Acoustic Radiation from an Airfoil in a Turbulent Stream," *Journal of Sound and Vibration*, Vol. 41, No. 4, 1975, pp. 407–420.

[2]Jacob, M. C., Boudet, J., Casalino, D., and Michard, M., "A rod-airfoil experiment as a benchmark for broadband noise modeling," *Theoretical and Computational Fluid Dynamics*, Vol. 19, 2005, pp. 171–196.

[3]Casalino, D., Jacob, M. C., and Roger, M., "Prediction of rod-airfoil interaction noise using the Ffowcs-Williams and Hawkings Analogy," *AIAA Journal*, Vol. 41, No. 2, 2003, pp. 182–191.

[4]Boudet, J., Grosjean, N., and Jacob, M. C., "Wake-airfoil interaction as broadband noise source: a large-eddy simulation study," *International Journal of Aeroacoustics*, Vol. 4, No. 1-2, 2005, pp. 93–116.

[5]Berland, J., Lafon, P., Crouzet, F., Daude, F., and Bailly, C., "Numerical insight into sound sources of a rod-airfoil flow configuration using direct noise calculation," *16th AIAA/CEAS Aeroacoustics Conference*, AIAA, 2010.

[6]Eltaweel, A. and Wang, M., "Numerical Simulation of Broadband Noise from Airfoil-Wake Interaction," *17th AIAA/CEAS Aeroacoustics Conference*, AIAA, 2011.

[7]Jean-Christophe Giret, Alois Sengissen, Stéphane Moreau, Marlène Sanjosé, and Jean-Christophe Jouhaud, "Prediction of the sound generated by a rod-airfoil configuration using a compressible unstructured LES solver and a FW-H analogy," *AIAA-2012-2058*, 18th AIAA/CEAS Conference, AIAA, 2012.

[8]Vreman, A. W., "An Eddy-Viscosity Subgrid-Scale Model for Turbulent Shear Flow: Algebraic Theory and Applications," *Physics of Fluids*, Vol. 16, No. 10, 2004, pp. 3670–3681.

[9]C. Kato and M. Ikegawa, "Large Eddy Simulation of Unsteady Turbulent Wake of a Circular Cylinder using the Finite Element Method," *Advances in Numerical Simulation of Turbulent Flows*, Vol. 1, 1991, pp. 49–56.